

Cite this: *Chem. Sci.*, 2025, 16, 13486 All publication charges for this article have been paid for by the Royal Society of ChemistryReceived 1st March 2025  
Accepted 20th June 2025

DOI: 10.1039/d5sc01637a

rsc.li/chemical-science

# Mechanistic insights into spontaneous redispersion of ZnO onto TiO<sub>2</sub> in water-containing environments†

Conghui Liu,<sup>ab</sup> Rongtan Li,<sup>b</sup> Xiaohui Feng,<sup>b</sup> Yuting Sun,<sup>b</sup> Yamei Fan,<sup>b</sup> Jiaxin Li<sup>b</sup> and Qiang Fu<sup>ab\*</sup>

Water has a profound effect on the surface structure and catalytic performance of numerous heterogeneous catalysts. Understanding the mechanism of structural evolution in water-containing reaction atmospheres is essential for the rational design of catalysts with enhanced catalytic efficiency and stability. In this work, we have observed spontaneous redispersion of physically mixed ZnO particles onto TiO<sub>2</sub> surfaces in water-containing environments at room temperature. Water vapor at a pressure greater than 3.2 kPa is a prerequisite for the efficient ZnO redispersion, in which a water adlayer with a thickness of about three monolayers forms on the TiO<sub>2</sub> surface. Raising the sample temperature to 50 °C or rendering the TiO<sub>2</sub> surface hydrophobic prevents the formation of the water adlayer and thereby inhibits the ZnO redispersion. Solid-state nuclear magnetic resonance spectroscopy and *in situ* spectroscopic analyses confirm that the surface water adlayer serves as a migration channel for ZnO species. Moreover, ZnO achieves more rapid and complete redispersion in a liquid water environment. This structural regulation strategy increases the number of exposed active sites in the ZnO–TiO<sub>2</sub> catalyst, leading to enhanced catalytic activity in propane dehydrogenation.

## Introduction

Solid catalysts frequently undergo structural modifications during both pretreatment and catalytic reactions.<sup>1–5</sup> Controlled structural evolution can generate new active structures and increase the number of active sites, thereby enhancing catalytic performance.<sup>6–9</sup> For example, Ag particles can redisperse into single atoms in O<sub>2</sub> at 400 °C, which exhibit improved activity in selective catalytic reduction of NO with C<sub>3</sub>H<sub>6</sub>.<sup>10,11</sup> In the propane dehydrogenation reaction at 550 °C, ZnO migrates and anchors on hydroxyl nests of the silicalite-1 support, forming a highly stable active structure.<sup>12,13</sup> However, uncontrollable changes, such as sintering,<sup>14–16</sup> over-oxidation,<sup>17,18</sup> phase transition,<sup>19,20</sup> and loss of active components,<sup>21,22</sup> typically degrade catalytic efficiency. Therefore, it is crucial to understand the effects of surrounding media on the structural evolution of catalysts in order to construct active structures and prevent deactivation of the operating catalysts.

Water, as one of the most ubiquitous substances, plays a significant role in the structural evolution of many catalysts.<sup>23,24</sup> For instance, introduction of H<sub>2</sub>O vapor into O<sub>2</sub> at 400

°C can promote redispersion of Ag and Cu nanoparticles supported on Al<sub>2</sub>O<sub>3</sub>.<sup>10,25</sup> H<sub>2</sub>O vapor can induce a stable strong metal–support interaction (SMSI) structure in the Au/TiO<sub>2</sub> catalyst at 600 °C, enhancing the catalyst stability in CO oxidation reaction.<sup>26</sup> In addition, H<sub>2</sub>O vapor can alter the chemical state of catalysts during high-temperature catalytic reactions, thereby promoting or inhibiting the catalytic processes.<sup>17,27,28</sup> Even at room temperature (RT), water vapor can induce structural evolution of supported catalysts.<sup>29,30</sup> For example, exposing the Ni/h-AlN catalyst to moist air at RT results in hydrolysis of AlN and further forms an SMSI structure.<sup>31</sup> Pretreatment of the Pd/SiO<sub>2</sub> catalyst in air containing 10% H<sub>2</sub>O leads to aggregation of Pd nanoparticles and catalyst deactivation during the formaldehyde oxidation reaction.<sup>29</sup> Liquid water medium may have even stronger structural regulation effect on many catalysts. The strong covalent metal–support interaction of Pt single-atom catalysts with CoFe<sub>2</sub>O<sub>4</sub> can be modulated by a simple water-soaking treatment, improving the catalytic activity of methane combustion.<sup>32</sup> Additionally, Ag clusters can aggregate to form large particles through Ostwald ripening in liquid water.<sup>33</sup> Although the influence of water on the structural evolution of catalysts is frequently observed, the underlying mechanisms remain to be explored in more detail.

In this study, we investigate the water effect on ZnO redispersion onto TiO<sub>2</sub> at RT. The degree of ZnO redispersion increases with the water content in water-containing gaseous environments. Solid-state nuclear magnetic resonance

<sup>a</sup>School of Chemistry, Dalian University of Technology, Dalian 116024, China<sup>b</sup>State Key Laboratory of Catalysis, Chinese Academy of Sciences, Dalian Institute of Chemical Physics, Dalian 116023, China. E-mail: qfu@dicp.ac.cn† Electronic supplementary information (ESI) available. See DOI: <https://doi.org/10.1039/d5sc01637a>

spectroscopy (NMR) and diffuse reflectance infrared Fourier transform spectroscopy (DRIFTS) studies demonstrate that the formation of a water adlayer with around three monolayer (ML) thickness on the TiO<sub>2</sub> surface is necessary for efficient ZnO redispersion, which requires water vapor pressure higher than 3.2 kPa at RT. Increasing H<sub>2</sub>O vapor partial pressure enhances the formation of a thicker water adlayer and accelerates the ZnO redispersion process, and the maximum redispersion rate is achieved in liquid water. Low treatment temperature and support surface hydrophilization facilitate the formation of a thicker water adlayer under the same conditions. In contrast, increasing the temperature causes the stronger evaporation of surface-adsorbed water, and the hydrophobic treatment of the support prevents the formation of the water adlayer, both of which inhibit ZnO redispersion. The water-induced redispersion significantly reduces the size of ZnO particles, presenting a new regeneration method for sintered supported catalysts and enhancing catalytic performance in propane dehydrogenation (PDH).

## Experimental

### Sample preparation

ZnO powder (Macklin) was physically mixed with anatase TiO<sub>2</sub> powder (Macklin) at a 1 : 20 mass ratio to prepare a 5 wt% ZnO–TiO<sub>2</sub> sample. The sample was then treated in a H<sub>2</sub>O/O<sub>2</sub> atmosphere, and the obtained sample was denoted as ZnO–TiO<sub>2</sub>–H<sub>2</sub>O. Additionally, the ZnO–TiO<sub>2</sub> sample was immersed in liquid water and subsequently dried to obtain the sample designated as ZnO–TiO<sub>2</sub>–Water. The same method was employed to deposit 5 wt% ZnO onto  $\gamma$ -Al<sub>2</sub>O<sub>3</sub> and SiO<sub>2</sub> supports with comparable specific surface areas, yielding 5 wt% ZnO–Al<sub>2</sub>O<sub>3</sub> and 5 wt% ZnO–SiO<sub>2</sub> catalysts. The corresponding samples after H<sub>2</sub>O/O<sub>2</sub> treatment were designated as ZnO–Al<sub>2</sub>O<sub>3</sub>–H<sub>2</sub>O and ZnO–SiO<sub>2</sub>–H<sub>2</sub>O.

Saturated H<sub>2</sub>O vapor was introduced into O<sub>2</sub> through a bubbler, and the resulting gas was denoted as 3.2% H<sub>2</sub>O/O<sub>2</sub>, where 3.2% refers to the proportion of 3.2 kPa H<sub>2</sub>O vapor in the atmosphere. The content of H<sub>2</sub>O vapor in the atmosphere was adjusted by mixing dry and moist O<sub>2</sub> in varying proportions. The resulting gases were denoted as 0.3% H<sub>2</sub>O/O<sub>2</sub> and 1.6% H<sub>2</sub>O/O<sub>2</sub> according to the proportion of H<sub>2</sub>O vapor in the atmosphere. Supersaturated H<sub>2</sub>O vapor in O<sub>2</sub> was generated by heating the bubbler to 40 °C, which was denoted as 7.4% H<sub>2</sub>O/O<sub>2</sub>.

TiO<sub>2</sub> was immersed and stirred in ammonia solution with concentrations of 28%, 14% and 3%, respectively, at RT for 12 h and then dried to produce TiO<sub>2</sub> with varying degrees of hydrophilicity.<sup>34</sup> Commercial hydrophobized TiO<sub>2</sub> (Macklin) was modified with stearic acid. ZnO was loaded onto the modified TiO<sub>2</sub> by physically mixing, producing samples designated as ZnO-hydrophilic TiO<sub>2</sub> and ZnO-hydrophobic TiO<sub>2</sub>, respectively.

### Characterization

Scanning transmission electron microscopy (STEM) images were acquired using a JEM-F200 high-resolution scanning

transmission electron microscope operated at 200 kV, which was equipped with an energy dispersive X-ray spectroscopy (EDS) for elemental analysis. X-ray diffraction (XRD) patterns were recorded on Empyrean-100 and SmartLab diffractometers using a Cu K $\alpha$  radiation source ( $\lambda = 1.5406$  Å) at a scanning rate of 10–20° min<sup>−1</sup>. The ZnO diffraction peak at 36.3° was used to assess the degree of ZnO redispersion by normalizing its intensity to the TiO<sub>2</sub> diffraction peak at 25.5° and recording it as  $I_{\text{ZnO}}/I_{\text{TiO}_2}$ .

X-ray photoelectron spectroscopy (XPS) analyses were conducted on a SPECS spectrometer with either an Al K $\alpha$  source (1486.6 eV) or a Mg K $\alpha$  source (1253.6 eV) operated at 300 W. *In situ* XPS experiments were performed on a laboratory-based SPECS near-ambient pressure XPS (NAP-XPS) system. ZnO–TiO<sub>2</sub> samples were heated to various temperatures in a 0.5 mbar H<sub>2</sub>O atmosphere, and then spectra were collected. The binding energies were calibrated using the C 1s peak at 284.8 eV. The Zn 2p peak was used as an indicator of the ZnO redispersion state,<sup>35,36</sup> and its intensity was normalized to the Ti 3d peak and recorded as  $A_{\text{Zn}2p}/A_{\text{Ti}3d}$ .

Solid-state NMR experiments were conducted using Bruker Avance NEO 400 MHz and Bruker Avance III 600 MHz NMR spectrometers, which are both equipped with a 4 mm H-X double resonance magic angle spinning (MAS) NMR probe. Single-pulse <sup>1</sup>H MAS NMR spectra were acquired at a spinning rate of 8 kHz with a  $\pi/2$  pulse length of 3.3 or 5  $\mu$ s. The chemical shifts for <sup>1</sup>H were referenced to adamantane at 1.74 ppm. The hydrogen amount in the samples was determined using polydimethylsiloxane (PDMS) as an external standard.

DRIFTS analysis was performed with a VERTEX 80V full-band high-resolution infrared spectrometer. *In situ* experiments were conducted by heating the sample to 450 °C in Ar for 1 h to remove surface adsorbates, then cooling it to the target temperature and exposing it to air containing 1.2% H<sub>2</sub>O until saturation was reached.

### Catalytic activity tests

The propane dehydrogenation reaction was evaluated using a microreactor connected to an Agilent 8890 gas chromatograph. A 0.20 g catalyst with 5 wt% ZnO loading in a quartz tube was heated to 550 °C in N<sub>2</sub> and then exposed to the reaction gas at the same temperature. The feed gas consisted of 5 vol% C<sub>3</sub>H<sub>8</sub>, 5 vol% Ar, N<sub>2</sub> balance and the total flow rate was 20 mL min<sup>−1</sup>. Weight hourly space velocity (WHSV) was 0.54 h<sup>−1</sup>. The products were analyzed using an online gas chromatograph equipped with a thermal conductivity detector (TCD) and a hydrogen flame ionization detector (FID).

The propane conversion and propylene selectivity were calculated as follows:

$$\text{C}_3\text{H}_8 \text{ conversion} = \frac{C_3\text{H}_{8\text{in}}^{\text{TCD}} - C_3\text{H}_{8\text{out}}^{\text{TCD}}}{C_3\text{H}_{8\text{in}}^{\text{TCD}}} \times 100\%$$

$$\text{C}_x\text{H}_y \text{ selectivity} = \frac{C_x\text{H}_{y\text{out}}^{\text{FID}} \times f}{\sum C_x\text{H}_{y\text{out}}^{\text{FID}} \times f} \times 100\%$$



$$C \text{ balance} = \frac{\sum C_x H_{\text{yout}}^{\text{FID}} \times f}{C_3 H_{8\text{in}}^{\text{FID}} - C_3 H_{8\text{out}}^{\text{FID}}} \times 100\%$$

Here, TCD and FID refer to the signal sources.  $C_x H_y$  represents all hydrocarbon species except  $C_3 H_8$ , and the symbol  $f$  stands for the relative correction factor. The inlet concentration is obtained using an empty tube test.

When investigating the effect of space velocity, feed gases containing 0.5 vol%, 1 vol%, and 40 vol%  $C_3 H_8$  were introduced while maintaining a constant flow rate of  $20 \text{ mL min}^{-1}$ . The pre-oxidation treatment involved heating the sample to  $550^\circ\text{C}$  at a ramp rate of  $10^\circ\text{C min}^{-1}$  under a  $40 \text{ mL min}^{-1}$   $O_2$  flow, followed by purging with  $100 \text{ mL min}^{-1}$   $N_2$  for 10 min prior to switching to the reaction gas. For catalyst regeneration, the used catalyst was exposed to  $40 \text{ mL min}^{-1}$   $O_2$  at the reaction temperature of  $550^\circ\text{C}$  for 10 min, after which the system was switched back to the reaction gas. During all gas switching procedures, a  $100 \text{ mL min}^{-1}$   $N_2$  purge was consistently applied for 10 min to prevent gas mixing. The reaction order of propane dehydrogenation with respect to propane was determined by analyzing the reaction kinetics under varying concentrations of propane in the feed gas. Additionally, the activation energies of the catalytic reaction were calculated for both pristine and water-treated catalysts by examining the temperature-dependent reaction profiles. All kinetic experiments were conducted under differential reaction conditions, maintaining  $C_3 H_8$  conversion below 10% to ensure kinetic control. The studies employed gas flow rates of 20 or  $40 \text{ mL min}^{-1}$ , with 2 vol%, 5 vol%, and 10 vol%  $C_3 H_8$  in the reactant gas.

## Results and discussion

### $H_2O$ -mediated spontaneous redispersion of ZnO onto the $TiO_2$ surface

The ZnO- $TiO_2$  sample with 5 wt% ZnO loading was prepared by physically mixing ZnO powder with anatase  $TiO_2$  powder. In the XRD pattern, the distinct diffraction peaks at  $31.8^\circ$ ,  $34.5^\circ$ , and  $36.3^\circ$  corresponding to the (100), (002) and (101) crystal planes of ZnO (PDF#75-0576) confirm the presence of ZnO particles in the ZnO- $TiO_2$  sample (Fig. 1a). After treatment in a 3.2%  $H_2O/O_2$  atmosphere at RT for 12 h (denoted as ZnO- $TiO_2$ - $H_2O$ ), the characteristic ZnO diffraction peaks almost disappear while  $TiO_2$  diffraction peaks still remain unchanged (Fig. 1a and S1a†), suggesting either reduction in the size or decrease in the number of ZnO particles. Raman spectra exhibit the absence of ZnO vibrational modes, while the characteristic bands of  $TiO_2$  also remain unaffected by the vapor treatment (Fig. S1b†). XPS results demonstrate a significant increase in the intensity of the Zn  $2p_{3/2}$  peak at 1021.8 eV (Fig. S1c†) and a 4.7-fold increase in the Zn 2p/ $Ti$  3d peak area ratio for the ZnO- $TiO_2$ - $H_2O$  sample (Fig. 1b), indicating enhanced dispersion degree of ZnO after  $H_2O$  vapor treatment.<sup>37</sup> STEM and EDS mapping images further reveal that most ZnO particles with sizes of hundreds of nanometers in the ZnO- $TiO_2$  sample (Fig. 1c) are no longer observable after the  $H_2O$  vapor treatment (Fig. 1d). The homogeneous

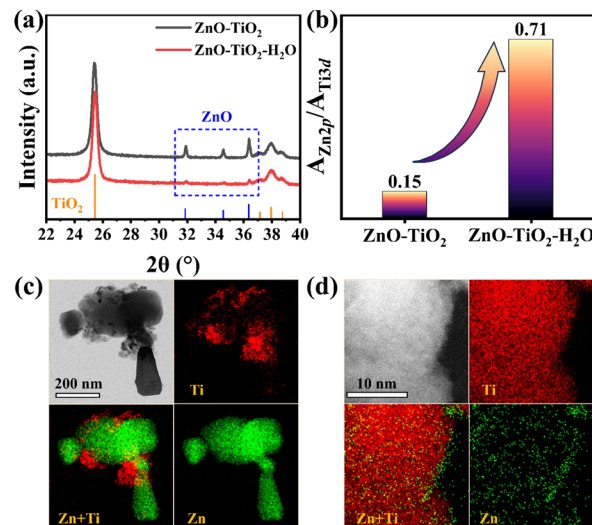


Fig. 1 Spontaneous redispersion of ZnO onto the  $TiO_2$  surface. (a) XRD patterns of ZnO- $TiO_2$  and ZnO- $TiO_2$ - $H_2O$  samples. (b) Zn 2p/ $Ti$  3d XPS peak area ratio of ZnO- $TiO_2$  and ZnO- $TiO_2$ - $H_2O$  samples. STEM and EDS mapping images of (c) ZnO- $TiO_2$  and (d) ZnO- $TiO_2$ - $H_2O$  samples.

distribution of Zn species across the  $TiO_2$  support, as evidenced by EDS mapping images, suggests that the original large ZnO particles have redispersed into nanoclusters or nanolayers on the  $TiO_2$  surface (Fig. 1d and S2†). These findings demonstrate that  $H_2O$  vapor treatment at ambient temperature can effectively induce spontaneous redispersion of ZnO onto  $TiO_2$ .

We further investigated ZnO redispersion onto different supports under water vapor treatment. For 5 wt% ZnO- $Al_2O_3$ , the ZnO diffraction peaks weaken significantly yet remain detectable after the treatment (Fig. S3a†), while 5 wt% ZnO- $SiO_2$  shows negligible changes (Fig. S3b†). The observed variation in ZnO dispersity on different supports with comparable surface areas likely originates from the distinct ZnO-support interaction strength.<sup>13,38</sup>

### Mechanism of $H_2O$ -mediated ZnO redispersion

To investigate the effect of  $H_2O$  content on ZnO redispersion, ZnO- $TiO_2$  samples were treated in  $O_2$  containing  $H_2O$  vapor with various partial pressures for 12 h and subsequently characterized using XRD and XPS. As shown in Fig. 2a, the intensity of ZnO diffraction peaks at  $31.8^\circ$ ,  $34.5^\circ$ , and  $36.3^\circ$  remains unchanged for the samples treated in 0.3% and 1.6%  $H_2O/O_2$ , indicating that these  $H_2O$  partial pressures are insufficient to induce the spontaneous redispersion of ZnO. However, increasing the  $H_2O$  content to 2.3%, 3.2% or 7.4% leads to noticeable weakening of ZnO diffraction peaks under identical treatment conditions. Correspondingly, the Zn 2p/ $Ti$  3d XPS peak area ratio of the sample treated in 1.6%  $H_2O/O_2$  remains close to the initial value of 0.24. In contrast, the ratio increases by 1.9-fold in 2.3%  $H_2O/O_2$ , 3.0-fold in 3.2%  $H_2O/O_2$  and by 3.7-fold in 7.4%  $H_2O/O_2$  (Fig. 2b), indicating that the higher  $H_2O$  vapor partial pressures promote the stronger ZnO redispersion. Moreover, when the ZnO- $TiO_2$  sample is directly immersed in



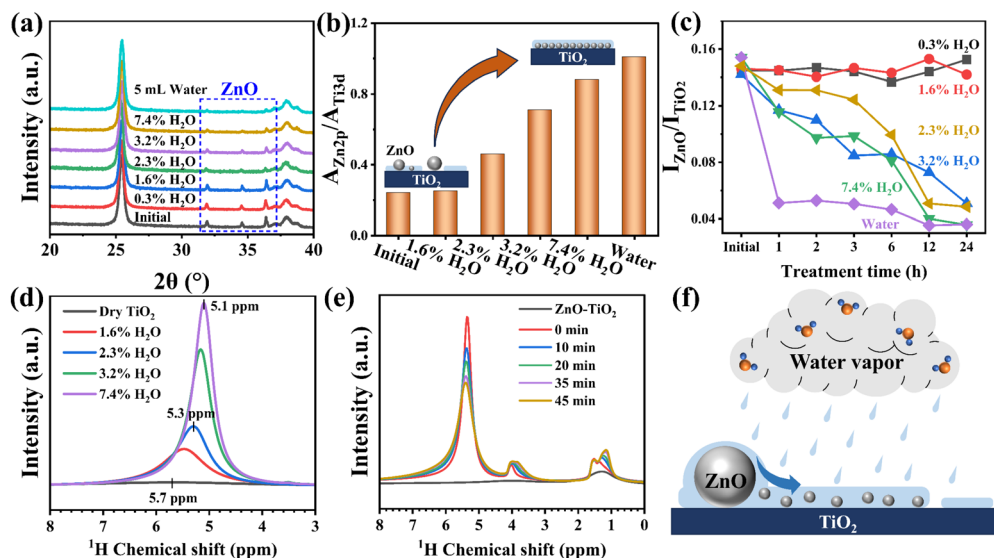


**Fig. 2** Effect of  $\text{H}_2\text{O}$  content on ZnO redispersion. (a) XRD patterns of ZnO–TiO<sub>2</sub> treated in  $\text{O}_2$  containing  $\text{H}_2\text{O}$  with various partial pressures for 12 h. (b) Zn 2p/Ti 3d XPS peak area ratios of ZnO–TiO<sub>2</sub> treated in  $\text{O}_2$  containing  $\text{H}_2\text{O}$  with various partial pressures for 12 h. (c) ZnO diffraction peak intensity of ZnO–TiO<sub>2</sub> treated in  $\text{O}_2$  containing  $\text{H}_2\text{O}$  with various partial pressures over time. (d)  $^1\text{H}$  NMR spectra of TiO<sub>2</sub> treated in  $\text{O}_2$  containing  $\text{H}_2\text{O}$  with various partial pressures for 3 h. (e) *In situ*  $^1\text{H}$  NMR spectra of ZnO–TiO<sub>2</sub> after introducing 10  $\mu\text{L}$  water without direct contact. (f) Schematic diagram of the formation of a water adlayer to promote ZnO redispersion onto TiO<sub>2</sub>.

liquid water for 12 h, the ZnO diffraction peaks nearly disappear, accompanied by a 4.2-fold increase in the Zn 2p/Ti 3d ratio (Fig. 2a and b), suggesting that ZnO redisperses more completely in liquid water. The minimal leaching of Zn species ( $6.08 \text{ mg L}^{-1}$  in filtrate) coupled with nearly constant Zn loading (3.76 wt%) in the ZnO–TiO<sub>2</sub> sample after water immersion demonstrates the absence of significant ZnO loss through dissolution. Complementary characterization by XRD and Raman further confirms that the structural integrity of TiO<sub>2</sub> remains unaltered in liquid water (Fig. S4†).

The relationship between the decrease rate of the ZnO diffraction peak intensity and the  $\text{H}_2\text{O}$  content in the gaseous atmosphere was assessed based on the XRD data. As shown in Fig. 2c, for the samples treated in 0.3% and 1.6%  $\text{H}_2\text{O}/\text{O}_2$ , the intensity of the ZnO diffraction peak at  $36.3^\circ$  remains unchanged over time. In contrast, the samples treated in 2.3%, 3.2% and 7.4%  $\text{H}_2\text{O}/\text{O}_2$  show a rapid and continuous decrease in ZnO peak intensity. Furthermore, for the sample immersed in liquid water, the ZnO peak intensity experiences an abrupt reduction within the first hour, followed by a gradual decrease over time. These time-dependent profiles indicate that  $\text{H}_2\text{O}$  content modulates both the extent and rate of ZnO redispersion.

To explore the mechanism of water-promoting ZnO redispersion,  $^1\text{H}$  NMR experiments were conducted on TiO<sub>2</sub> samples.<sup>39</sup> Fig. 2d shows a weak peak at 5.7 ppm in the  $^1\text{H}$  NMR spectra of dry TiO<sub>2</sub>, corresponding to hydrogen atoms in surface adsorbed water on TiO<sub>2</sub>.<sup>40,41</sup> Upon treatment in  $\text{O}_2$  with increasing  $\text{H}_2\text{O}$  contents for 3 h, the peak becomes more pronounced and shifts to the high-frequency region (5.1 ppm), indicating that the content of adsorbed water on TiO<sub>2</sub> increases with the  $\text{H}_2\text{O}$  partial pressure in the gaseous environment.

Quantitative analysis using internal standards reveals that adsorbed water coverage increases from 0.2 ML on dry TiO<sub>2</sub> to 1.2 ML after 1.6%  $\text{H}_2\text{O}/\text{O}_2$  treatment (Table S1†) while ZnO redispersion has not been observed under these conditions. The average water coverage on TiO<sub>2</sub> treated in 2.3%, 3.2% and 7.4%  $\text{H}_2\text{O}/\text{O}_2$  reaches 1.7, 2.8 and 3.2 ML, respectively, in which cases ZnO redispersion starts to occur. This correlation suggests that a sufficient water adlayer thickness is required to facilitate the efficient migration and redispersion of ZnO. Previous molecular dynamics simulations demonstrate that the outermost water layer in the three layers of adsorbed water on the TiO<sub>2</sub> surface exhibits the highest mobility compared to inner layers,<sup>42–45</sup> potentially enabling ZnO transport through this hydrated interface.<sup>33,46,47</sup>

*In situ* solid-state NMR experiments were performed to observe the temporal evolution of water adlayer formation on TiO<sub>2</sub>. Different volumes of liquid water were introduced into the closed rotor without contacting the TiO<sub>2</sub> sample, but allowing  $\text{H}_2\text{O}$  molecules to adsorb onto the TiO<sub>2</sub> surface through vapor phase transport. The initial spectrum shows a single peak at 5.6 ppm, corresponding to protons in the primary interfacial water (Fig. S5†), which is directly in contact with and strongly bound to TiO<sub>2</sub>.<sup>40</sup> As the water volume increases, a new peak emerges at 4.9 ppm and becomes increasingly pronounced, which is attributed to mobile outer-layer water molecules interacting with the primary interfacial  $\text{H}_2\text{O}$  and OH groups through weaker hydrogen bonds.<sup>45,48</sup> The area ratio of these two peaks ( $A_{4.9 \text{ ppm}}/A_{5.6 \text{ ppm}}$ ) increases from 0 to 2.0 as the water amount increases, demonstrating preferential accumulation of the outer-layer water. It is noteworthy that the  $^1\text{H}$  NMR peak of outer-layer water (4.9 ppm) gradually weakens over time, while the peaks corresponding to interfacial water (5.6 ppm) and



hydroxyl groups (1.1 ppm) show an increase in intensity (Fig. S6†). This spectral evolution suggests continuous structural reorganization of the water adlayer, where outer-layer water transforms into interfacial water and hydroxyl groups.<sup>40</sup> The presence of merged signals in Fig. 2d reflects equilibrium between these dynamic processes, ultimately forming an interconnected hydrogen-bond network.<sup>45</sup>

*In situ* solid-state NMR experiments were performed on the ZnO–TiO<sub>2</sub> sample to observe the interaction between H<sub>2</sub>O and ZnO. After introducing 10  $\mu$ L water into the closed rotor without the direct contact between the water and the catalyst, the <sup>1</sup>H NMR spectrum shows the presence of a strong H<sub>2</sub>O peak (5.4 ppm), a hydroxyl signal (1.1 ppm) and a peak at 3.9 ppm (Fig. 2e) identified as Zn–H species.<sup>49–52</sup> Over time, the water signal progressively decreases while both the hydroxyl and Zn–H signals increase (Fig. 2e), providing the direct evidence of ZnO-promoted water dissociation and the strong interaction between ZnO and H<sub>2</sub>O. This ZnO redispersion process controlled by the water adlayer is illustrated in Fig. 2f.

### Tuning ZnO redispersion by temperature or surface modification

As shown above, treatment in 3.2% H<sub>2</sub>O/O<sub>2</sub> at RT for 12 h leads to the redispersion of ZnO onto TiO<sub>2</sub>, as evidenced by the disappearance of ZnO diffraction peaks. However, when the treatment temperature increases from 20 to 50 °C under the identical 3.2% H<sub>2</sub>O/O<sub>2</sub> conditions, the ZnO diffraction peaks exhibit progressively enhanced intensities (Fig. S7a†). At 50 °C and above, ZnO diffraction peaks remain almost unchanged (Fig. 3a). XPS results reveal that the Zn 2p/Ti 3d peak area ratio of the ZnO–TiO<sub>2</sub> sample increases 4.8-fold after treatment in

3.2% H<sub>2</sub>O/O<sub>2</sub> at RT, but shows no significant change when treated at 50 °C (Fig. S7b†). These results demonstrate that elevated temperatures have an inhibitory effect on the spontaneous redispersion of ZnO in water-containing gaseous environments.

To probe this temperature-dependent phenomenon, the surface hydration states of TiO<sub>2</sub> were examined using solid-state NMR, DRIFTS and *in situ* XPS. The <sup>1</sup>H NMR spectrum of ZnO–TiO<sub>2</sub> treated in 3.2% H<sub>2</sub>O/O<sub>2</sub> at 25 °C displays substantially stronger adsorbed water signals compared to the sample treated at 50 °C (Fig. 3b). Quantitative calculations indicate that the adsorbed water amount on TiO<sub>2</sub> in 3.2% H<sub>2</sub>O/O<sub>2</sub> at 50 °C is limited to 0.2 ML. DRIFTS spectra further confirm this trend, where the H<sub>2</sub>O peak at 3400 cm<sup>−1</sup> (H–O stretching vibration peak of H<sub>2</sub>O molecule<sup>53</sup>) shows negligible intensity variation between TiO<sub>2</sub> treated in H<sub>2</sub>O/O<sub>2</sub> at 50 °C and TiO<sub>2</sub> without water treatment (Fig. 3c). In contrast, the TiO<sub>2</sub> treated in H<sub>2</sub>O/O<sub>2</sub> at 25 °C exhibits markedly stronger absorption. *In situ* DRIFTS spectra shown in Fig. S7c† indicate that as the temperature decreases, the H<sub>2</sub>O peak in the DRIFTS spectrum becomes stronger when the TiO<sub>2</sub> surface is saturated with adsorption in air containing 1.2% H<sub>2</sub>O. *In situ* O 1s XPS spectra of the ZnO–TiO<sub>2</sub> sample show that exposure to 0.5 mbar H<sub>2</sub>O atmosphere at RT increases both hydroxyl group content and adsorbed water signals (533.2 eV),<sup>54,55</sup> but the adsorbed water peak disappears upon heating to 50 °C (Fig. 3d). Collectively, the fact that high temperatures hinder ZnO redispersion is attributed to the suppressed formation of a water adlayer on the TiO<sub>2</sub> surface.

When ZnO–TiO<sub>2</sub> is immersed in liquid water at 90 °C for 3 h, XRD analysis shows complete disappearance of ZnO diffraction peaks (Fig. S7d†), demonstrating that elevated temperatures do

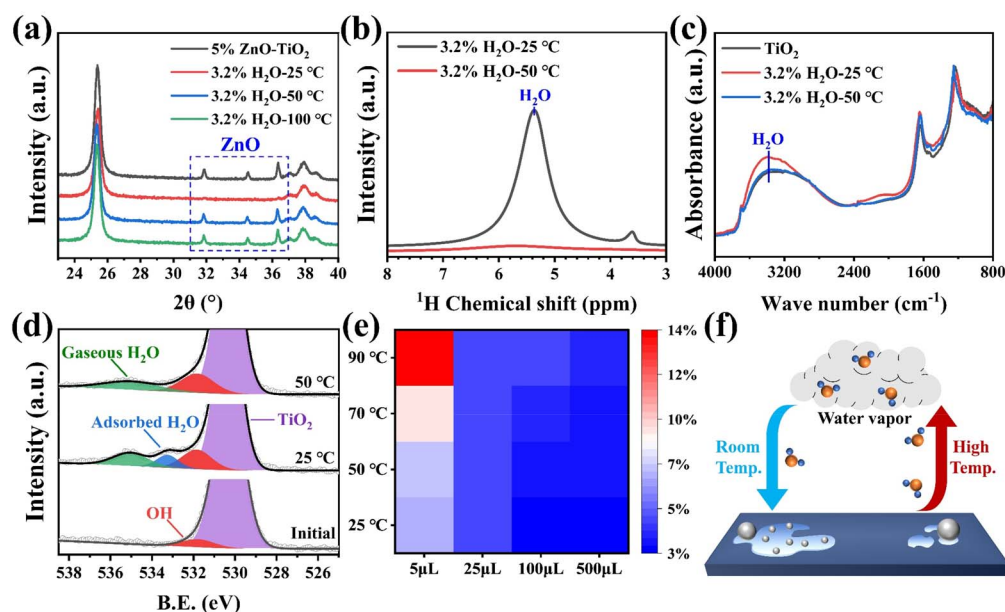


Fig. 3 Effect of temperature on ZnO redispersion. (a) XRD patterns of ZnO–TiO<sub>2</sub> before and after treatment in 3.2% H<sub>2</sub>O/O<sub>2</sub> at different temperatures. (b) <sup>1</sup>H NMR and (c) DRIFTS spectra of ZnO–TiO<sub>2</sub> after treatment in 3.2% H<sub>2</sub>O/O<sub>2</sub> at RT and 50 °C. (d) *In situ* O 1s XPS spectra of the ZnO–TiO<sub>2</sub> sample in a 0.5 mbar H<sub>2</sub>O atmosphere at different temperatures. (e) Heat map of the diffraction peak intensity of ZnO at 36.3° in Fig. S5.† (f) Schematic diagram of the temperature-influenced ZnO redispersion process.



not inhibit ZnO redispersion in aqueous environments, in contrast to the gas-phase behavior. To investigate this contrast with gas-phase behavior, a 0.1 g ZnO–TiO<sub>2</sub> sample was placed in a 10 mL sealed bottle, and varying volumes of liquid water were introduced without direct contact with the sample. Then, these bottles were treated at different temperatures for 12 h and XRD analyses were conducted on the samples (Fig. S8†). The intensity variations of ZnO diffraction peaks at 36.3° are visualized as a heat map (Fig. 3e), which clearly demonstrates that elevated temperatures (50–90 °C) inhibit ZnO redispersion at low water volumes (5 µL), whereas this inhibitory effect diminishes when water quantity exceeds 25 µL. This temperature-dependent behavior primarily originates from different water evaporation rates at various temperatures (Table S2†). By correlating the average adsorbed water coverage with water evaporation behavior at different temperatures, we establish the temperature-dependent water requirements for ZnO redispersion in this system (Fig. S9†). These findings establish that temperature primarily modulates ZnO redispersion through its influence on adsorbed water availability under the evaporation–condensation equilibrium, rather than directly affecting reaction kinetics. The process of temperature-influenced ZnO redispersion is schematically illustrated in Fig. 3f.

Based on these findings, the possibility of surface chemical modification strategies to regulate ZnO redispersion was explored.<sup>56–58</sup> TiO<sub>2</sub> was pretreated with 28 wt% ammonia solution to enhance its hydrophilicity,<sup>34</sup> achieving a water contact

angle of 10.1° *versus* 16.8° for untreated TiO<sub>2</sub> (Fig. 4a). When hydrophilic TiO<sub>2</sub> is employed for ZnO redispersion in 3.2% H<sub>2</sub>O/O<sub>2</sub>, ZnO diffraction peaks also significantly weaken, and XPS analysis demonstrates an increased Zn 2p/Ti 3d peak area ratio of 0.93 (Fig. 4b and c), exceeding the ratio of 0.71 observed with untreated TiO<sub>2</sub>. Furthermore, a decrease in the concentration of used ammonia solution (14 wt% and 3 wt%) leads to reduction in the Zn 2p/Ti 3d ratio (0.82 and 0.77, respectively) after H<sub>2</sub>O/O<sub>2</sub> treatment (Fig. 4c). In contrast, TiO<sub>2</sub> modified with stearic acid exhibits hydrophobic characteristics, having a water contact angle of 113.8° (Fig. 4a). XRD patterns reveal that ZnO diffraction peaks of the ZnO–hydrophobic TiO<sub>2</sub> sample remain unchanged after H<sub>2</sub>O/O<sub>2</sub> treatment (Fig. 4d), indicating that ZnO cannot spontaneously redisperse onto hydrophobic TiO<sub>2</sub>. The wetting property of the hydrophobic TiO<sub>2</sub> has been controlled by calcining at different temperatures, which is followed by ZnO loading and H<sub>2</sub>O/O<sub>2</sub> treatment. The calcination at 100 or 200 °C has little effect on the XRD pattern and Zn 2p/Ti 3d ratio (Fig. 4d and e). After calcination at 300 °C, the ZnO diffraction peak intensity decreases but remains clearly detectable after H<sub>2</sub>O/O<sub>2</sub> treatment, and the Zn 2p/Ti 3d ratio increases from 0.09 to 0.50 (Fig. 4d and e), indicating limited redispersion of ZnO. The results establish a direct correlation between TiO<sub>2</sub> hydrophilicity and ZnO redispersion efficiency.

Solid-state <sup>1</sup>H NMR was used to quantify the adsorbed water on the surface-modified TiO<sub>2</sub>. After the treatment in 3.2% H<sub>2</sub>O/O<sub>2</sub>, hydrophilic TiO<sub>2</sub> retains 3.2 ML of adsorbed water, slightly

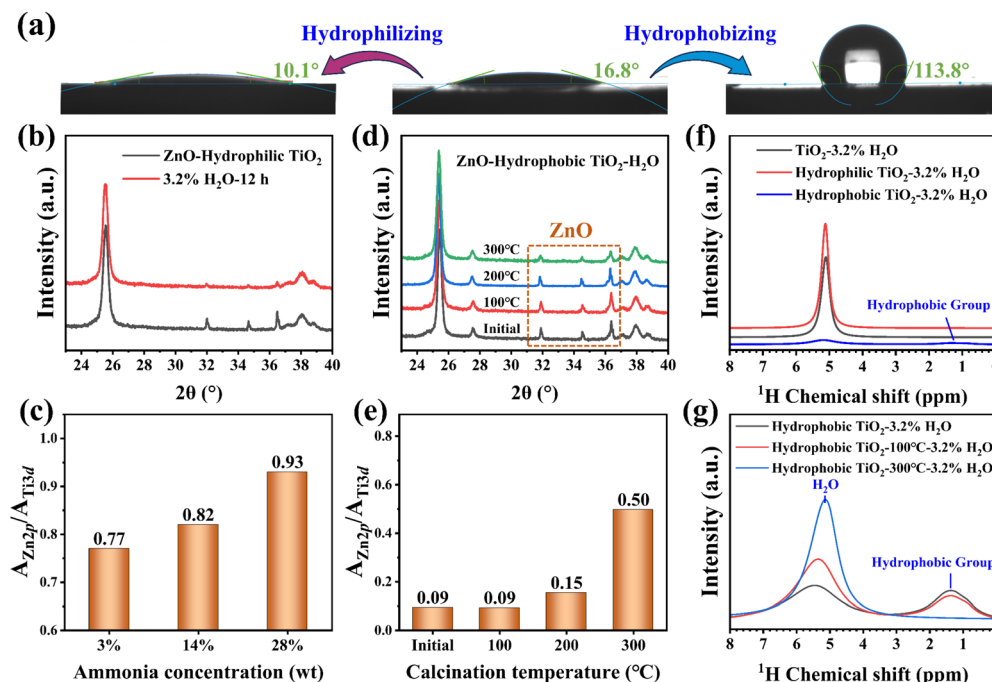


Fig. 4 Effect of support hydrophilicity and hydrophobicity on ZnO redispersion. (a) Contact angle measurement of water on fresh TiO<sub>2</sub>, hydrophilic TiO<sub>2</sub> and hydrophobic TiO<sub>2</sub> samples. (b) XRD patterns of ZnO–hydrophilic TiO<sub>2</sub> before and after treatment in 3.2% H<sub>2</sub>O/O<sub>2</sub>. (c) Zn 2p/Ti 3d XPS peak area ratio of ZnO mixed with TiO<sub>2</sub> hydrophilized in ammonia solution with different concentrations and after H<sub>2</sub>O/O<sub>2</sub> treatment. (d) XRD patterns and (e) Zn 2p/Ti 3d XPS peak area ratios of ZnO mixed with hydrophobic TiO<sub>2</sub> calcined at different temperatures and after treatment in 3.2% H<sub>2</sub>O/O<sub>2</sub>. (f) <sup>1</sup>H NMR spectra of TiO<sub>2</sub>, hydrophilic TiO<sub>2</sub>, and hydrophobic TiO<sub>2</sub> samples after treatment in 3.2% H<sub>2</sub>O/O<sub>2</sub>. (g) <sup>1</sup>H NMR spectra of hydrophobic TiO<sub>2</sub> calcined at different temperatures and after treatment in 3.2% H<sub>2</sub>O/O<sub>2</sub>.

exceeding 2.8 ML on untreated TiO<sub>2</sub>. In contrast, hydrophobic TiO<sub>2</sub> exhibits a drastically reduced water adsorption capacity of 0.4 ML under identical conditions (Fig. 4f). <sup>1</sup>H NMR spectra further demonstrate that increasing the calcination temperature of hydrophobic TiO<sub>2</sub> progressively reduces the peak intensity of surface hydrophobic groups while enhancing the water adlayer peak after H<sub>2</sub>O/O<sub>2</sub> treatment (Fig. 4g). Quantitative analysis reveals that hydrophobic TiO<sub>2</sub> calcined at 300 °C achieves only 0.9 ML of surface water coverage after H<sub>2</sub>O/O<sub>2</sub> treatment. DRIFTS analysis corroborates these trends, where the O–H stretching vibration at 3400 cm<sup>−1</sup> for hydrophobic TiO<sub>2</sub> remains less intense than that of untreated TiO<sub>2</sub> even after H<sub>2</sub>O/O<sub>2</sub> treatment (Fig. S10†). These findings suggest that hydrophilic modification facilitates thicker water adlayer formation under the same conditions, thereby enhancing ZnO redispersion. Conversely, hydrophobic modification inhibits water adsorption, restricting water adlayer thickness below the critical threshold required for ZnO migration and redispersion. This systematic comparison conclusively demonstrates the indispensable role of outer-layer water in mediating ZnO redispersion.

### Catalytic activity test

Propane dehydrogenation serves as a vital industrial process for propylene production. Zinc-based catalysts offer significant advantages in this process due to their low cost and environmental friendliness. To evaluate the impact of ZnO redispersion on catalytic activity, PDH activities of ZnO–TiO<sub>2</sub> samples were compared before and after H<sub>2</sub>O treatment. As illustrated in Fig. 5a, the initial C<sub>3</sub>H<sub>8</sub> conversion over ZnO–TiO<sub>2</sub>–H<sub>2</sub>O is

significantly higher than that of ZnO–TiO<sub>2</sub>, while C<sub>3</sub>H<sub>6</sub> selectivity remains similar in a wide temperature range (Fig. S11†). Through kinetic analysis of PDH activity at varying temperatures and propane partial pressures, it is confirmed that the propane dehydrogenation reaction follows pseudo-first-order kinetics with respect to propane (Fig. S12†) and the activation energy of the PDH reaction remains essentially unchanged before and after water treatment of the catalyst (Fig. 5b). Therefore, the increase in C<sub>3</sub>H<sub>8</sub> conversion of the ZnO–TiO<sub>2</sub> sample at 550 °C from 5.8% to 48.2% (8.3-fold enhancement) after water treatment mainly correlates with increased exposure of Zn–O active sites through the water-induced redispersion. ZnO–TiO<sub>2</sub>–H<sub>2</sub>O demonstrates notable catalytic performance for propane dehydrogenation among many Zn-based catalysts (Fig. 5c and Table S3†).<sup>12,13,59–66</sup> However, the catalyst rapidly deactivates due to ZnO consumption and carbon deposition under reductive conditions (Fig. S13a†). To improve stability, pre-oxidation (heating in 40 mL min<sup>−1</sup> O<sub>2</sub>) or regeneration (550 °C, 40 mL min<sup>−1</sup> O<sub>2</sub>, 10 min) is applied. Although initial conversion decreases from 48.2% to 26.8%, the ZnO–TiO<sub>2</sub>–H<sub>2</sub>O catalyst retains catalytic activity above 25% over 1 h operation with multiple regeneration cycles (Fig. 5d). Compared with the samples prepared by the impregnation method, the ZnO–TiO<sub>2</sub>–H<sub>2</sub>O catalyst consistently shows higher conversion and propylene space-time yield (STY) than 5% ZnO/TiO<sub>2</sub> (Fig. S13b†). In particular, after pre-oxidation or regeneration treatment and reaction for 40 min, the ZnO–TiO<sub>2</sub>–H<sub>2</sub>O catalyst retains a C<sub>3</sub>H<sub>8</sub> conversion of ~28% with a propylene STY of 0.13 g<sub>C<sub>3</sub>H<sub>6</sub></sub> h<sup>−1</sup> g<sub>cat</sub><sup>−1</sup>, outperforming the 5% ZnO/TiO<sub>2</sub> catalyst (~20% conversion, 0.09 g<sub>C<sub>3</sub>H<sub>6</sub></sub> h<sup>−1</sup> g<sub>cat</sub><sup>−1</sup>).

## Conclusions

This work establishes a water-mediated strategy for structural regulation of ZnO/TiO<sub>2</sub> catalysts. Through multiple characterization techniques, we demonstrate that ZnO spontaneously redisperses into nanoclusters or nanolayers on TiO<sub>2</sub> in the presence of water. The redispersion of ZnO is attributed to its strong interaction with TiO<sub>2</sub> and is influenced by the content of water present in the environment. Solid-state NMR analysis quantitatively correlates this phenomenon with water adlayer thickness, revealing that nearly 3 monolayers of adsorbed water generate sufficient outer-layer regions to enable efficient ZnO redispersion. Based on this understanding, increasing the temperature above 50 °C can limit the water adlayer to below 0.2 ML, and hydrophobically modifying TiO<sub>2</sub> also produces the adlayer with a coverage of 0.4 ML, both of which can completely inhibit the spontaneous redispersion of ZnO. The controlled regulation of ZnO size ultimately enhances the performance of the ZnO–TiO<sub>2</sub> catalyst in the propane dehydrogenation reaction, increasing C<sub>3</sub>H<sub>8</sub> conversion by more than 8-fold and retaining propylene selectivity above 95%.

## Data availability

The data that support the findings of this study are available within the article and the ESI.†

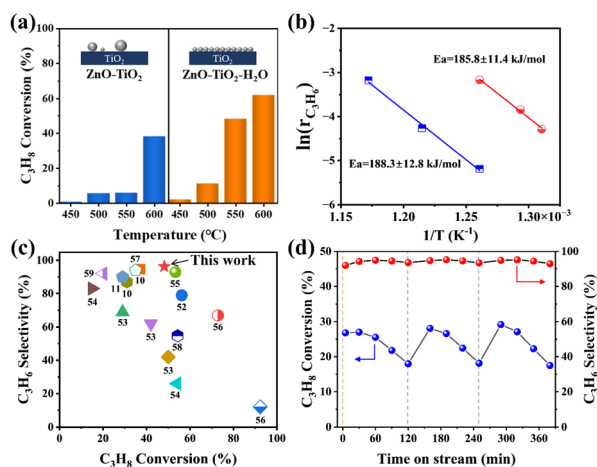


Fig. 5 Catalytic performance. (a) C<sub>3</sub>H<sub>8</sub> conversion in the PDH reaction at different temperatures for ZnO–TiO<sub>2</sub> before and after H<sub>2</sub>O treatment. Reaction conditions: 5 vol% C<sub>3</sub>H<sub>8</sub>, 5 vol% Ar, N<sub>2</sub> balance; WHSV = 0.54 h<sup>−1</sup>. (b) Arrhenius plots for the calculation of the apparent activation energy of the propane dehydrogenation reaction over ZnO–TiO<sub>2</sub> catalysts. (c) Comparison of PDH performance of Zn-based catalysts in this work and other studies.<sup>12,13,59–66</sup> (d) Stability test of the ZnO–TiO<sub>2</sub>–H<sub>2</sub>O catalyst in the PDH reaction after pre-oxidation and regeneration (orange dashed line: pre-oxidation process, heating to 550 °C in 40 mL min<sup>−1</sup> O<sub>2</sub>; gray dashed line: regeneration process, treatment in 40 mL min<sup>−1</sup> O<sub>2</sub> at 550 °C for 10 min).



## Author contributions

Q. F. conceived the project. C. L. and R. L. designed the studies. X. F. guided catalytic experiments. Y. S. performed NMR experiments. R. L. performed the *in situ* XPS experiment. C. L. performed other experiments. C. L., R. L., Y. F. and J. L. analyzed all the experimental data. C. L., R. L. and Q. F. wrote the manuscript. All authors interpreted the data and contributed to the preparation of the manuscript.

## Conflicts of interest

There are no conflicts to declare.

## Acknowledgements

This work was financially supported by the National Key R&D Program of China (2021YFA1502800, 2022YFA1504800 and 2022YFA1504500), National Natural Science Foundation of China (21825203, 22288201, 22332006 and 22321002), Fundamental Research Funds for the Central Universities (20720220009), Photon Science Center for Carbon Neutrality, and Dalian Innovation Support Plan for High Level Talents (2023RG002).

## References

- 1 L. Piccolo, Restructuring effects of the chemical environment in metal nanocatalysis and single-atom catalysis, *Catal. Today*, 2021, **373**, 80–97.
- 2 Z.-P. Wu, S. Shan, S.-Q. Zang and C.-J. Zhong, Dynamic Core-Shell and Alloy Structures of Multimetallic Nanomaterials and Their Catalytic Synergies, *Acc. Chem. Res.*, 2020, **53**, 2913–2924.
- 3 S. Zhao, Y. Yang and Z. Tang, Insight into Structural Evolution, Active Sites, and Stability of Heterogeneous Electrocatalysts, *Angew. Chem., Int. Ed.*, 2022, **61**, e202110186.
- 4 B. Zhu, J. Meng, W. Yuan, X. Zhang, H. Yang, Y. Wang and Y. Gao, Reshaping of Metal Nanoparticles Under Reaction Conditions, *Angew. Chem., Int. Ed.*, 2019, **59**, 2171–2180.
- 5 W. Tan, S. Xie, X. Zhang, K. Ye, M. Almousawi, D. Kim, H. Yu, Y. Cai, H. Xi, L. Ma, S. N. Ehrlich, F. Gao, L. Dong and F. Liu, Fine-Tuning of Pt Dispersion on Al<sub>2</sub>O<sub>3</sub> and Understanding the Nature of Active Pt Sites for Efficient CO and NH<sub>3</sub> Oxidation Reactions, *ACS Appl. Mater. Interfaces*, 2024, **16**, 454–466.
- 6 Z. W. Seh, J. Kibsgaard, C. F. Dickens, I. Chorkendorff, J. K. Nørskov and T. F. Jaramillo, Combining theory and experiment in electrocatalysis: Insights into materials design, *Science*, 2017, **355**, eaad4998.
- 7 W. Huang, A. C. Johnston-Peck, T. Wolter, W. D. Yang, L. Xu, J. Oh, B. A. Reeves, C. Zhou, M. E. Holtz, A. A. Herzing, A. M. Lindenberg, M. Mavrikakis and M. Cargnello, Steam-created grain boundaries for methane C-H activation in palladium catalysts, *Science*, 2021, **373**, 1518–1523.
- 8 M. Chen, B. Wu, J. Yang and N. Zheng, Small Adsorbate-Assisted Shape Control of Pd and Pt Nanocrystals, *Adv. Mater.*, 2012, **24**, 862–879.
- 9 B. Zhang, J. Yang, Y. Mu, X. Ji, Y. Cai, N. Jiang, S. Xie, Q. Qian, F. Liu, W. Tan and L. Dong, Fabrication of Highly Dispersed Ru Catalysts on CeO<sub>2</sub> for Efficient C<sub>3</sub>H<sub>6</sub> Oxidation, *Environ. Sci. Technol.*, 2024, **58**, 19533–19544.
- 10 C. Liu, R. Li, F. Wang, K. Li, Y. Fan, R. Mu and Q. Fu, Water promoted structural evolution of Ag nanocatalysts supported on alumina, *Nano Res.*, 2023, **16**, 9107–9115.
- 11 F. Wang, J. Z. Ma, S. H. Xin, Q. Wang, J. Xu, C. B. Zhang, H. He and X. C. Zeng, Resolving the puzzle of single-atom silver dispersion on nanosized  $\gamma$ -Al<sub>2</sub>O<sub>3</sub> surface for high catalytic performance, *Nat. Commun.*, 2020, **11**, 529.
- 12 D. Zhao, X. Tian, D. E. Doronkin, S. Han, V. A. Kondratenko, J. D. Grunwaldt, A. Perechodjuk, T. H. Vuong, J. Rabeah, R. Eckelt, U. Rodemerck, D. Linke, G. Jiang, H. Jiao and E. V. Kondratenko, In situ formation of ZnO<sub>x</sub> species for efficient propane dehydrogenation, *Nature*, 2021, **599**, 234–238.
- 13 D. Zhao, K. Guo, S. Han, D. E. Doronkin, H. Lund, J. Li, J.-D. Grunwaldt, Z. Zhao, C. Xu, G. Jiang and E. V. Kondratenko, Controlling Reaction-Induced Loss of Active Sites in ZnO<sub>x</sub>/Silicalite-1 for Durable Nonoxidative Propane Dehydrogenation, *ACS Catal.*, 2022, **12**, 4608–4617.
- 14 S. B. Duan, R. M. Wang and J. Y. Liu, Stability investigation of a high number density Pt<sub>1</sub>/Fe<sub>2</sub>O<sub>3</sub> single-atom catalyst under different gas environments by HAADF-STEM, *Nanotechnology*, 2018, **29**, 204002.
- 15 Y. Nishihata, J. Mizuki, T. Akao, H. Tanaka, M. Uenishi, M. Kimura, T. Okamoto and N. Hamada, Self-regeneration of a Pd-perovskite catalyst for automotive emissions control, *Nature*, 2002, **418**, 164–167.
- 16 J.-S. Lee and J.-H. Yu, Diffusion-Controlled Grain Growth in Liquid-Phase Sintering of W-Cu Nanocomposites, *Int. J. Mater. Res.*, 2001, **92**, 663–668.
- 17 J. Zhu, P. Wang, X. Zhang, G. Zhang, R. Li, W. Li, T. P. Senftle, W. Liu, J. Wang, Y. Wang, A. Zhang, Q. Fu, C. Song and X. Guo, Dynamic structural evolution of iron catalysts involving competitive oxidation and carburization during CO<sub>2</sub> hydrogenation, *Sci. Adv.*, 2022, **8**, eabm3629.
- 18 Y. Yazawa, N. Kagi, S.-i. Komai, A. Satsuma, Y. Murakami and T. Hattori, Kinetic study of support effect in the propane combustion over platinum catalyst, *Catal. Lett.*, 2001, **72**, 157–160.
- 19 G. Chen, R. Wang, W. Zhao, B. Kang, D. Gao, C. Li and J. Y. Lee, Effect of Ru crystal phase on the catalytic activity of hydrolytic dehydrogenation of ammonia borane, *J. Power Sources*, 2018, **396**, 148–154.
- 20 A. N. Pour and M. Housaindokht, Effects of metallic cobalt crystal phase on catalytic activity of cobalt catalysts supported on carbon nanotubes in Fischer-Tropsch synthesis, *Prog. React. Kinet. Mech.*, 2019, **44**, 316–323.
- 21 P. Gallezot, P. J. Cerino, B. Blanc, G. Flèche and P. Fuertes, Glucose hydrogenation on promoted raney-nickel catalysts, *J. Catal.*, 1994, **146**, 93–102.





- 22 M. Besson and P. Gallezot, Selective oxidation of alcohols and aldehydes on metal catalysts, *Catal. Today*, 2000, **57**, 127–141.
- 23 A. Goguet, R. Burch, Y. Chen, C. Hardacre, P. Hu, R. W. Joyner, F. C. Meunier, B. S. Mun, D. Thompson and D. Tibiletti, Deactivation Mechanism of a Au/CeZrO<sub>4</sub> Catalyst During a Low-Temperature Water Gas Shift Reaction, *J. Phys. Chem. C*, 2007, **111**, 16927–16933.
- 24 D. Li, F. Xu, X. Tang, S. Dai, T. Pu, X. Liu, P. Tian, F. Xuan, Z. Xu, I. E. Wachs and M. Zhu, Induced activation of the commercial Cu/ZnO/Al<sub>2</sub>O<sub>3</sub> catalyst for the steam reforming of methanol, *Nat. Catal.*, 2022, **5**, 99–108.
- 25 A. A. Liu, L. C. Liu, Y. Cao, J. M. Wang, R. Si, F. Gao and L. Dong, Controlling dynamic structural transformation of atomically dispersed CuO<sub>x</sub> species and influence on their catalytic performances, *ACS Catal.*, 2019, **9**, 9840–9851.
- 26 H. Wang, X. Dong, Y. Hui, Y. Niu, B. Zhang, L. Liu, J. Cao, M. Yabushita, Y. Nakagawa, K. Tomishige, Y. Qin, L. Song, J. Xiao, L. Wang and F.-S. Xiao, Oxygen-Saturated Strong Metal-Support Interactions Triggered by Water on Titania Supported Catalysts, *Adv. Funct. Mater.*, 2023, **33**, 2304303.
- 27 J. Dong, Q. Fu, H. Li, J. Xiao, B. Yang, B. Zhang, Y. Bai, T. Song, R. Zhang, L. Gao, J. Cai, H. Zhang, Z. Liu and X. Bao, Reaction-Induced strong metal-support interactions between metals and inert boron nitride nanosheets, *J. Am. Chem. Soc.*, 2020, **142**, 17167–17174.
- 28 M. Wang, P. Wang, G. Zhang, Z. Cheng, M. Zhang, Y. Liu, R. Li, J. Zhu, J. Wang, K. Bian, Y. Liu, F. Ding, T. P. Senftle, X. Nie, Q. Fu, C. Song and X. Guo, Stabilizing Co<sub>2</sub>C with H<sub>2</sub>O and K promoter for CO<sub>2</sub> hydrogenation to C<sub>2+</sub> hydrocarbons, *Sci. Adv.*, 2023, **9**, eadg0167.
- 29 C. Wang, J. Wang, X. Liu, Y. Li, C. Zhang, Y. Zheng and W. Shan, Abnormal inhibiting effect of H<sub>2</sub>O on Pd/SiO<sub>2</sub> and Na-Pd/SiO<sub>2</sub> catalysts for HCHO oxidation, *Catal. Sci. Technol.*, 2023, **13**, 6409–6414.
- 30 Y. Fan, R. Li, B. Wang, X. Feng, X. Du, C. Liu, F. Wang, C. Liu, C. Dong, Y. Ning, R. Mu and Q. Fu, Water-assisted oxidative redispersion of Cu particles through formation of Cu hydroxide at room temperature, *Nat. Commun.*, 2024, **15**, 3046.
- 31 S. Li, Y. Fu, W. Kong, B. Pan, C. Yuan, F. Cai, H. Zhu, J. Zhang and Y. Sun, Dually confined Ni nanoparticles by room-temperature degradation of AlN for dry reforming of methane, *Appl. Catal., B*, 2020, **277**, 118921.
- 32 J. Yang, Y. Huang, H. Qi, C. Zeng, Q. Jiang, Y. Cui, Y. Su, X. Du, X. Pan, X. Liu, W. Li, B. Qiao, A. Wang and T. Zhang, Modulating the strong metal-support interaction of single-atom catalysts via vicinal structure decoration, *Nat. Commun.*, 2022, **13**, 4244.
- 33 C. Liu, R. Li, Y. Fan, S. Li, X. Feng, L. Feng, Y. Ning and Q. Fu, Liquid-mediated Ostwald ripening of Ag-based clusters supported on oxides, *Nano Res.*, 2024, **17**, 4971–4978.
- 34 Q. Kang, G. Li, Z. Li, Y. Tian and C. Wang, Surface co-hydrophilization via ammonia inorganic strategy for low-temperature Cu/SiO<sub>2</sub> hybrid bonding, *J. Mater. Sci. Technol.*, 2023, **149**, 161–166.
- 35 A. M. Tarditi, M. F. Mori and L. M. Cornaglia, Determination of the Metal Dispersion of Supported Catalysts Using XPS, *Top. Catal.*, 2019, **62**, 822–837.
- 36 Z. D. Davis and B. J. Tatarchuk, Understanding the dispersion of Ag on high surface area TiO<sub>2</sub> supports using XPS intensity ratios, *Appl. Surf. Sci.*, 2015, **353**, 679–685.
- 37 R. Li, X. Xu, B. Zhu, X. Y. Li, Y. Ning, R. Mu, P. Du, M. Li, H. Wang, J. Liang, Y. Chen, Y. Gao, B. Yang, Q. Fu and X. Bao, In situ identification of the metallic state of Ag nanoclusters in oxidative dispersion, *Nat. Commun.*, 2021, **12**, 1406.
- 38 C. Dong, R. Li, Z. Qu, Y. Fan, J. Wang, X. Du, C. Liu, X. Feng, Y. Ning, R. Mu, Q. Fu and X. Bao, Oxide Support Inert in Its Interaction with Metal but Active in Its Interaction with Oxide and Vice Versa, *J. Am. Chem. Soc.*, 2025, **147**, 13210–13219.
- 39 J. Soria, J. Sanz, I. Sobrados, J. M. Coronado, A. J. Maira, M. D. Hernández-Alonso and F. Fresno, FTIR and NMR Study of the Adsorbed Water on Nanocrystalline Anatase, *J. Phys. Chem. C*, 2007, **111**, 10590–10596.
- 40 L. Yang, M. Huang, N. Feng, M. Wang, J. Xu, Y. Jiang, D. Ma and F. Deng, Unraveling the atomic structure and dissociation of interfacial water on anatase TiO<sub>2</sub>(101) under ambient conditions with solid-state NMR spectroscopy, *Chem. Sci.*, 2024, **15**, 11902–11911.
- 41 K. Oka, T. Shibue, N. Sugimura, Y. Watabe, B. Winther-Jensen and H. Nishide, Long-lived water clusters in hydrophobic solvents investigated by standard NMR techniques, *Sci. Rep.*, 2019, **9**, 223.
- 42 S. M. Rau, R. J. Hirsch, M. Junige, A. S. Cavanagh, A. L. P. Rotondaro, H. Paddubrouskaya, K. H. Abel and S. M. George, Strongly and Weakly Adsorbed H<sub>2</sub>O Layer Thicknesses on Hydroxylated SiO<sub>2</sub> Surfaces versus H<sub>2</sub>O Pressure at Various Substrate Temperatures, *J. Phys. Chem. C*, 2025, **129**, 1666–1677.
- 43 H. Li, M. Abdelgaid, J. R. Paudel, N. P. Holzapfel, V. Augustyn, J. R. McKone, G. Mpourmpakis and E. J. Crumlin, Operando Unveiling of Hydrogen Spillover Mechanisms on Tungsten Oxide Surfaces, *J. Am. Chem. Soc.*, 2025, **147**, 6472–6479.
- 44 D. B. Asay and S. H. Kim, Evolution of the Adsorbed Water Layer Structure on Silicon Oxide at Room Temperature, *J. Phys. Chem. B*, 2005, **109**, 16760–16763.
- 45 A. Y. Nosaka, T. Fujiwara, H. Yagi, H. Akutsu and Y. Nosaka, Characteristics of Water Adsorbed on TiO<sub>2</sub> Photocatalytic Systems with Increasing Temperature as Studied by Solid-State <sup>1</sup>H NMR Spectroscopy, *J. Phys. Chem. B*, 2004, **108**, 9121–9125.
- 46 F. Kraushofer, L. Haager, M. Eder, A. Rafsanjani-Abbasi, Z. Jakub, G. Franceschi, M. Riva, M. Meier, M. Schmid, U. Diebold and G. S. Parkinson, Single Rh adatoms stabilized on  $\alpha$ -Fe<sub>2</sub>O<sub>3</sub>(1-102) by coadsorbed water, *ACS Energy Lett.*, 2022, **7**, 375–380.
- 47 R. D. Glover, J. M. Miller and J. E. Hutchison, Generation of metal nanoparticles from silver and copper objects: nanoparticle dynamics on surfaces and potential sources



- of nanoparticles in the environment, *ACS Nano*, 2011, **5**, 8950–8957.
- 48 A. Y. Nosaka, E. Kojima, T. Fujiwara, H. Yagi, H. Akutsu and Y. Nosaka, Photoinduced Changes of Adsorbed Water on a TiO<sub>2</sub> Photocatalytic Film As Studied by <sup>1</sup>H NMR Spectroscopy, *J. Phys. Chem. B*, 2003, **107**, 12042–12044.
  - 49 D. Y. Ong, Z. Yen, A. Yoshii, J. Revillo Imbernon, R. Takita and S. Chiba, Controlled Reduction of Carboxamides to Alcohols or Amines by Zinc Hydrides, *Angew. Chem.*, 2019, **131**, 5046–5051.
  - 50 F. Ritter, T. P. Spaniol, I. Douair, L. Maron and J. Okuda, Molecular Zinc Hydride Cations [ZnH]<sup>+</sup>: Synthesis, Structure, and CO<sub>2</sub> Hydrosilylation Catalysis, *Angew. Chem., Int. Ed.*, 2020, **59**, 23335–23342.
  - 51 M. Tüchler, L. Gärtner, S. Fischer, A. D. Boese, F. Belaj and N. C. Mösch-Zanetti, Efficient CO<sub>2</sub> Insertion and Reduction Catalyzed by a Terminal Zinc Hydride Complex, *Angew. Chem.*, 2018, **130**, 7022–7025.
  - 52 F. Ritter, L. J. Morris, K. N. McCabe, T. P. Spaniol, L. Maron and J. Okuda, Deaggregation of Zinc Dihydride by Lewis Acids Including Carbon Dioxide in the Presence of Nitrogen Donors, *Inorg. Chem.*, 2021, **60**, 15583–15592.
  - 53 J. Szanyi, J. H. Kwak, R. J. Chimentao and C. H. F. Peden, Effect of H<sub>2</sub>O on the Adsorption of NO<sub>2</sub> on γ-Al<sub>2</sub>O<sub>3</sub>: an in Situ FTIR/MS Study, *J. Phys. Chem. C*, 2007, **111**, 2661–2669.
  - 54 S. Benkoulou, O. Sublemontier, M. Patanen, C. Nicolas, F. Sirotti, A. Naitabdi, F. Gaie-Levrel, E. Antonsson, D. Aureau, F.-X. Ouf, S.-I. Wada, A. Etcheberry, K. Ueda and C. Miron, Water adsorption on TiO<sub>2</sub> surfaces probed by soft X-ray spectroscopies: bulk materials vs. isolated nanoparticles, *Sci. Rep.*, 2015, **5**, 15088.
  - 55 A. Braun, F. Aksoy Akgul, Q. Chen, S. Erat, T.-W. Huang, N. Jabeen, Z. Liu, B. S. Mun, S. S. Mao and X. Zhang, Observation of Substrate Orientation-Dependent Oxygen Defect Filling in Thin WO<sub>3-δ</sub>/TiO<sub>2</sub> Pulsed Laser-Deposited Films with in Situ XPS at High Oxygen Pressure and Temperature, *Chem. Mater.*, 2012, **24**, 3473–3480.
  - 56 H. Zhang, H. Sun, D. Zhang, W. Zhang, S. Chen, M. Li and P. Liang, Nanoconfinement of Ag nanoparticles inside mesoporous channels of MCM-41 molecule sieve as a regenerable and H<sub>2</sub>O resistance sorbent for Hg<sup>0</sup> removal in natural gas, *Chem. Eng. J.*, 2019, **361**, 139–147.
  - 57 W. Yu, X. Yu and S.-T. Tu, Oxidation of Hydrogen Off-gas from a Fuel Cell Using a Microstructured Reactor with Hydrophobic Pt-Al<sub>2</sub>O<sub>3</sub> Catalyst Coating, *Energy Procedia*, 2014, **61**, 2854–2857.
  - 58 Y. Xu, X. Li, J. Gao, J. Wang, G. Ma, X. Wen, Y. Yang, Y. Li and M. Ding, A hydrophobic FeMn@Si catalyst increases olefins from syngas by suppressing C1 by-products, *Science*, 2021, **371**, 610–613.
  - 59 C. Chen, M. Sun, Z. Hu, J. Ren, S. Zhang and Z.-Y. Yuan, New insight into the enhanced catalytic performance of ZnPt/HZSM-5 catalysts for direct dehydrogenation of propane to propylene, *Catal. Sci. Technol.*, 2019, **9**, 1979–1988.
  - 60 S. M. T. Almutairi, B. Mezari, P. C. M. M. Magusin, E. A. Pidko and E. J. M. Hensen, Structure and Reactivity of Zn-Modified ZSM-5 Zeolites: The Importance of Clustered Cationic Zn Complexes, *ACS Catal.*, 2011, **2**, 71–83.
  - 61 T. Gong, L. Qin, J. Lu and H. Feng, ZnO modified ZSM-5 and Y zeolites fabricated by atomic layer deposition for propane conversion, *Phys. Chem. Chem. Phys.*, 2016, **18**, 601–614.
  - 62 C. Chen, Z. Hu, J. Ren, S. Zhang, Z. Wang and Z.-Y. Yuan, ZnO Nanoclusters Supported on Dealuminated Zeolite β as a Novel Catalyst for Direct Dehydrogenation of Propane to Propylene, *ChemCatChem*, 2019, **11**, 868–877.
  - 63 C. Chen, Z.-P. Hu, J.-T. Ren, S. Zhang, Z. Wang and Z.-Y. Yuan, ZnO supported on high-silica HZSM-5 as efficient catalysts for direct dehydrogenation of propane to propylene, *Mol. Catal.*, 2019, **476**, 110508.
  - 64 G. Liu, L. Zeng, Z.-J. Zhao, H. Tian, T. Wu and J. Gong, Platinum-Modified ZnO/Al<sub>2</sub>O<sub>3</sub> for Propane Dehydrogenation: Minimized Platinum Usage and Improved Catalytic Stability, *ACS Catal.*, 2016, **6**, 2158–2162.
  - 65 F. Zhang, C. Miao, Y. Yue, W. Hua and Z. Gao, Dehydrogenation of Propane to Propylene in the Presence of CO<sub>2</sub> over Steaming-treated HZSM-5 Supported ZnO, *Chin. J. Chem.*, 2012, **30**, 929–934.
  - 66 Y. Chai, S. Chen, Y. Chen, F. Wei, L. Cao, J. Lin, L. Li, X. Liu, S. Lin, X. Wang and T. Zhang, Dual-Atom Catalyst with N-Colligated Zn<sub>1</sub>Co<sub>1</sub> Species as Dominant Active Sites for Propane Dehydrogenation, *J. Am. Chem. Soc.*, 2024, **146**, 263–273.

